PAPER

NJC
www.rsc.org/njc

The generation of mesostructured crystalline CeO_2, ZrO_2 and CeO_2–ZrO_2 films using evaporation-induced self-assembly†

Torsten Brezesinski, Markus Antonietti,* Matthijs Groenewolt, Nicola Pinna and Bernd Smarsly

Max Planck Institute of Colloids and Interfaces, Research Campus Golm, D-14424 Potsdam, Germany. E-mail: pape@mpikg.mpg.de; Fax: +49-331-567-9502; Tel: +49-331-567-9501

Received (in Montpellier, France) 9th August 2004, Accepted 23rd September 2004
First published as an Advance Article on the web 8th December 2004

Mesostructured thin films of CeO_2, $ZrO_2$and CeO_2–ZrO_2 mixed oxides with highly crystalline pore walls and ordered arrays of mesopores were obtained by a straightforward fabrication process employing evaporation-induced self-assembly (EISA) and a well-designed temperature treatment, taking advantage of a novel type of amphiphilic block copolymer as template. The mesostructure and crystallinity were studied in detail using small-angle and wide-angle X-ray scattering and electron microscopy. The mesostructured CeO_2 films are crack-free, possess a final pore size of *ca.* 10 nm, and the mesopores are surrounded by an almost completely crystalline matrix of nanoparticles of *ca.* 5–7 nm in size, as revealed by high-resolution electron microscopy. Additionally, the mesoscopic order (bcc structure) shows high thermal stability. The crystallization of the walls is usually accompanied by stresses and strong uniaxial structural shrinkage, which can, however, be significantly diminished by making mixed CeO_2–ZrO_2 mesostructured systems. Here, the crystallites represent "solid solutions" of both binary oxides and exhibit an even higher thermal stability, while the constituting nanocrystals are smaller compared to the pure CeO_2.

Introduction

Recent progress in the synthesis of mesoporous materials by *in situ* characterization of the complex kinetic processes involved and their optimization,[1] as well as the development of more suitable and more "phase-robust" block copolymer templates,[2] has enabled the synthesis of essentially fully crystalline mesoporous titania[3] and diverse perovskite films.[4] As a further advantage, both the mesopore size (*ca.* 10 nm) and the thickness of the crystalline walls (*ca.* 6–10 nm) were tuned to be significantly larger compared to those obtained previous studies, thus leading to improved physicochemical properties and mechanical stability. For the first time, this new type of mesoporous material allows the study of dielectric and other properties as a function of the nanoparticle size. The resulting films, fabricated by the "evaporation-induced self-assembly" (EISA) process,[5] were shown to have good optical quality and to possess a uniform tunable thickness between 100 and 500 nm, so that they could be employed directly for the respective purpose of the functional oxides, *e.g.* for sensors or solar energy conversion.

Several studies report the fabrication of mesoporous crystalline ceria. However, usually the ceria mesostructure undergoes a severe breakdown throughout the final crystallization step,[6a–c] leading to rather ill-defined porosity without controlled nanocrystallinity in the pore walls in terms of the spatial distribution and the size of the oxide nanocrystals. For instance, Morris *et al.* reported the preparation of crystalline mesoporous ceria,[6d] but the pore size was rather small (*ca.* 2 nm) and the nanocrystals quite large, pointing to mesostructural collapse and a leftover intergrain porosity. In general, in previous reports the conclusion that the crystalline regions, detected by X-ray diffraction, originate from polycrystalline mesopore walls and not from non-porous domains created by mesostructural collapse remains ambiguous. Since in all cases small template molecules were used, the mesostructural collapse in these studies can be attributed to the geometric incompatibility of the primary nanocrystal size and the mesopore size determined by the template, in other words one cannot set up a finer tectonic with larger crystals. Just recently, Ozin *et al.* reported on an yttria-stabilized ZrO_2 as a solid oxide fuel cell electrode material, which, however, underwent heavy sintering throughout crystallization.[7] Sanchez *et al.* reported the first successful procedure to generate mesostructured ZrO_2–CeO_2 (rich in Zr) thin films using Pluronics polymers as a template.[8] To the best of our knowledge, no well-defined mesoporous structures (*e.g.* with cylindrical or spherical pore shape) of pure crystalline CeO_2 thin films and films with at least a balanced CeO_2/ZrO_2 ratio have been reported so far.

The continued search for a procedure to make pure mesoporous CeO_2 films or mixed CeO_2–ZrO_2 species with improved structural characteristics is motivated by the interesting functional properties of these materials.[9] Compared to other metal oxides, ceria and zirconia are known to be chemically and thermally extraordinarily stable and therefore used as catalyst supports and in ceramic membranes for catalysis and sensing.[9,10] In particular, mesoporous CeO_2 is highly interesting for redox processes and control over the nanocrystallite size on the nanometer scale was reported to optimize sensing properties.[10g]

Ceria only has one polymorph (a cubic fluorite structure) and in this structure it can easily switch between Ce^{4+} and Ce^{3+}, balancing the charge difference with oxygen vacancies; that is it can mediate oxidation. This distinct property makes it highly attractive in high-temperature solid oxide fuel cells. In general, CeO_2 based systems have been extensively studied and excellent reviews are available, which discuss different aspects from structural properties to catalytic application.[11] The

† Electronic supplementary information (ESI) available: SAXS of ZrO_2 films; AFM and SEM images of CeO_2 films; WAXS and SAXS for mixed ZrO_2 and CeO_2 films. See http://www.rsc.org/suppdata/nj/b4/b412306a/

DOI: 10.1039/b412306a

Table 1 Chemical composition of the initial solution and critical temperatures of crystallization and mesostructure degradation

	CeO_2	ZrO_2	CeO_2–ZrO_2
KLE/g	0.075	0.090	0.090
M1/g	0.875 ($CeCl_3 \cdot 7H_2O$)	0.5 ($ZrCl_4$)	0.480 ($CeCl_3 \cdot 7H_2O$)
M2/g	—	—	0.3 ($ZrCl_4$)
EtOH/g	7.59	7.59	8.86
THF/g	1.12	—	—
H_2O/g	0.2	0.7	0.4
Crystallization/°C	250	450	350
Mesostructural collapse/°C	>660	>650	>700

binary system CeO_2–ZrO_2 exhibits solid solution formation over a wide range of compositions.[8] Doping of zirconia with ceria stabilizes its tetragonal and cubic phases at room temperature.

It is the purpose of the present paper to describe the conditions under which thin films with mesopores of up to 10 nm can be fabricated using evaporation-induced self-assembly, starting from metal chloride solutions, and to characterize their structural features in detail by transmission electron microscopy (TEM), high resolution TEM (HRTEM), and small- and wide-angle X-ray scattering (SAXS and WAXS). As one of the key aspects, a novel block copolymer template is used, which significantly facilitates both the self-assembly process and the pore wall crystallization with preservation of the mesostructure.

By thorough X-ray diffraction study of the development of the crystallinity in the pore walls and the mesostructural changes as a function of the heat treatment, it is possible to optimize the mesopore structure and crystallinity simultaneously. Minimization of structural shrinkage by optimized processing and structural adjustment of template and primary nanocrystal size allow, in addition, flat crack-free films, which are required for most applications, to be obtained.

Experimental

Film processing and treatment

The starting inorganic precursors were $CeCl_3 \cdot 7H_2O$ and $ZrCl_4$. The block copolymer $H(CH_2CH_2CH_2(CH)CH_2CH_3)_{89}(OCH_2CH_2)_{79}OH$ (referred to as KLE) was used as surfactant template, which was prepared in our institute by anionic polymerization, the details being reported in ref. 2. The initial solutions were prepared by dissolving inorganic precursor into the selected solvent, before the block copolymer template KLE was added with the proper amount of EtOH–THF to dissolve it (*cf.* Table 1). The mesoporous thin films were prepared by dip-coating at constant withdrawal speed (6 mm s^{-1}) and constant relative humidity (10–20%). For CeO_2 a fast transfer to a chamber at 200 °C directly after dip-coating is necessary to prevent local crystallization of $CeCl_3 \cdot 7H_2O$. Stabilization of networks before crystallization was achieved by thermal consolidation (dehydration) at 300 °C under air for 60 min. The desired materials were obtained through controlled crystallization provided by heating with a ramp of 3 °C min^{-1} under air up to 660 °C for CeO_2, 650 °C for ZrO_2 and 700 °C for CeO_2–ZrO_2.

Film characterization

The WAXS experiments and SAXS measurements in reflection were performed using a D8 diffractometer from Bruker Instruments (wavelength 0.154 nm). A Philips CM200 FEG microscope, 200 kV, equipped with a field emission gun was used for HRTEM. Transmission electron microscopy images with high contrast were taken with a Zeiss EM 912 Ω at an acceleration voltage of 120 kV. The GISAXS experiments were carried out at the synchrotron beamline at ELETTRA (Trieste, Italy) at the SAXS beamline of the Austrian Academy of Sciences.

Results and discussion

Mesostructured CeO_2

As pointed out recently,[1,3] the fabrication of mesostructured films of metal oxides with optical quality requires the precise control of parameters such as the external humidity, solvent, dip-coating speed, *etc.* As one of its major advantages, the KLE polymer employed in the present set of experiments appeared to be less sensitive to changes in these parameters. However, each metal oxide still needs optimized fabrication conditions, depending on the special nature of the metal salts used. Compared to our recent work on titania,[3] the films have to be exposed to an elevated temperature (*ca.* 200 °C) directly (within seconds) after dip-coating, otherwise $CeCl_3 \cdot 7H_2O$ crystallization takes place (indicated by film turbidity) and the mesostructure is lost. The suitability of the KLE polymer for rapid self-assembly turned out to be essential in this step, thereby avoiding the insufficient build-up or loss of mesostructure usually observed in previous studies. In this respect, the present fabrication procedure is different from that for TiO_2 mesostructured films, reported recently.[1a,3] In these studies, the fabrication involved a slow heating ramp and pretreatment in the amorphous state, prior to crystallization. We believe that in the case of CeO_2 a fast heat treatment is needed to remove the major portion of the formed HCl and immobilize the

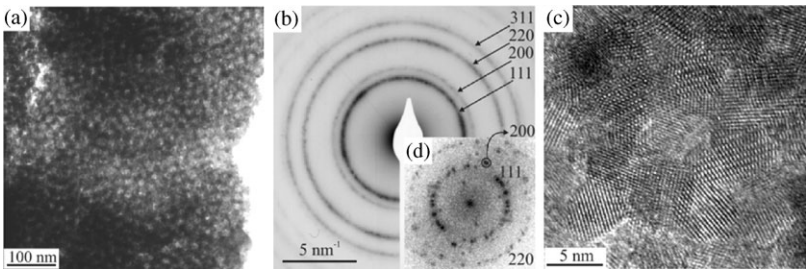

Fig. 1 (a) TEM image of a ceria film and (b) HRTEM, selected area electron diffraction of a zone of 250 nm diameter. (c) HRTEM image of a zone of 20 nm side length and (d) the power spectrum.

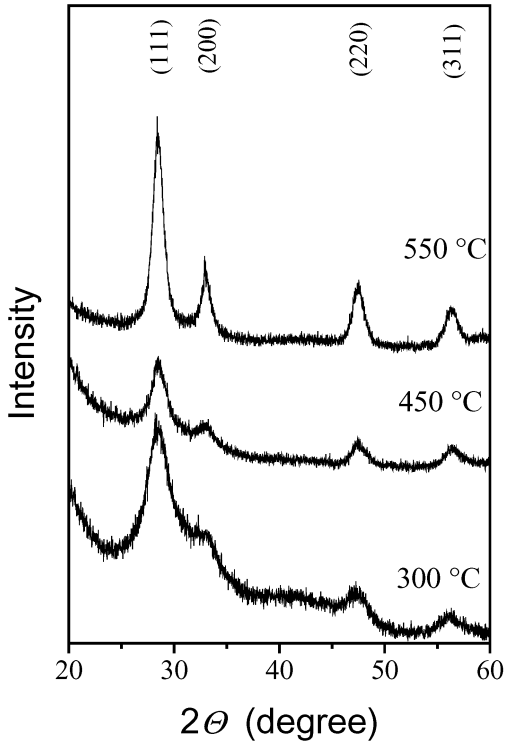

Fig. 2 WAXS diffractograms of the pure ceria film, obtained after annealing at different temperatures.

mesostructure, directly leading to partly crystalline CeO_2. The relatively harsh conditions for CeO_2 compared to the procedure reported by Sanchez *et al.* are not harmful to the mesostructure because of the slower crystallization rate of ceria.

Transmission electron microscopy (TEM) on films removed from the Si support demonstrates the high quality of the generated mesostructure. Fig. 1 depicts a pure ceria film, indicating that it is homogeneously mesoporous throughout large domains. The film thickness is *ca.* 170–200 nm, as determined by spectral ellipsometry.

The TEM images are consistent with a cubic array of spherical pores with an average diameter of about 9–10 nm, as determined on the basis of different TEM images. Also, this morphology is in full agreement with our previous work on mesoporous silica and titania, performed with the same block copolymer template.[2,3] In particular, the pore morphology is similar to the cubic distorted structure with connected mesopores observed recently in TiO_2 mesostructured films.[1a]

High resolution TEM of the same sample provides a more detailed view of the construction principle. Selected area electron diffraction [SAED; Fig. 1(b)] of such a zone displays diffraction rings characteristic of a structure composed of small domains with crystallographic axes randomly oriented with respect to each other. The *d* spacings measured from the diffraction rings are in good agreement with the cerianite structure (JCPDS 34-394). HRTEM of a square with 20 nm sides [Fig. 1(c)] shows several nanocrystallites with well-defined lattice planes, proving the high crystallinity of the sample. From such pictures, the primary nanocrystallite size is estimated to be about 6–8 nm and no significant amorphous fraction between the single particles could be identified. The crystallites are randomly oriented towards each other, as seen from the lattice fringes. This is further demonstrated by the power spectrum (PS) of this image [Fig. 1(d)], which is smeared out to narrow rings without preferential orientation. It is also seen that the pore size (*ca.* 10 nm) is larger than the primary crystal size, which is a crucial prerequisite for the mechanical stability of the mesopore framework. Taking into account the reported problems to obtain crystalline mesostructured ceria, our case seems to represent a borderline case where the crystallite and template size are still in a range that the mesostructure is maintained during the crystallization. Larger primary nanocrystals (as would result from a lower nucleation or growth rate) would certainly destroy the present mesopore structure and reconstitution to a porous powder material with an interstitial pore system would take place.

WAXS measurements performed after the different steps of the temperature treatment confirm the TEM results (Fig. 2). At 300 °C, the pure ceria system already shows a certain degree of crystallinity but with small nanoparticles of *ca.* 2 nm and coexisting amorphous regions. Treating the sample to 450 °C completes crystallization and after treatment for 10 min at 550 °C the WAXS peaks correspond to a primary crystal size of 7.6 nm, as calculated from the Scherrer equation. From the WAXS data of the sample treated at 550 °C it can be inferred that the maximum content of amorphous ceria is low and probably on the order of only several per cent. An exact determination was not possible, mainly because the density of the amorphous portions is unknown. The limited growth of the nanocrystals, even at high temperatures, is a prerequisite to maintain the mesopore structure.

The mesostructure was furthermore studied by both grazing incidence small-angle X-ray scattering (GISAXS) and SAXS in symmetric reflection as a function of the heat treatment (Fig. 3). While GISAXS in combination with a 2D detector allows the study of the mesostructure orientation, SAXS in symmetric reflection only shows the interferences in the *z* direction (lattice planes parallel to the substrate). It is remarkable that the mesostructure is still present at 600–650 °C, as revealed by GISAXS. The GISAXS pattern is indicative of a distorted bcc structure in the [110] orientation, as observed

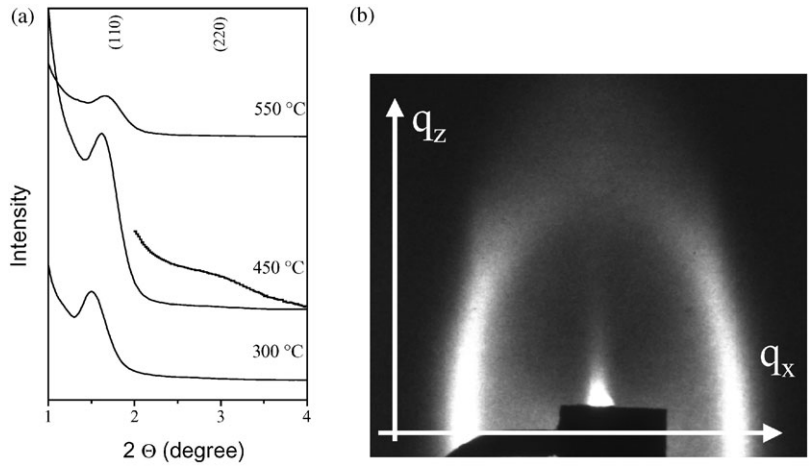

Fig. 3 (a) 1D SAXS (reflection) as a function of temperature treatment and (b) GISAXS (taken at 600 °C) of mesostructured CeO_2 thin films.

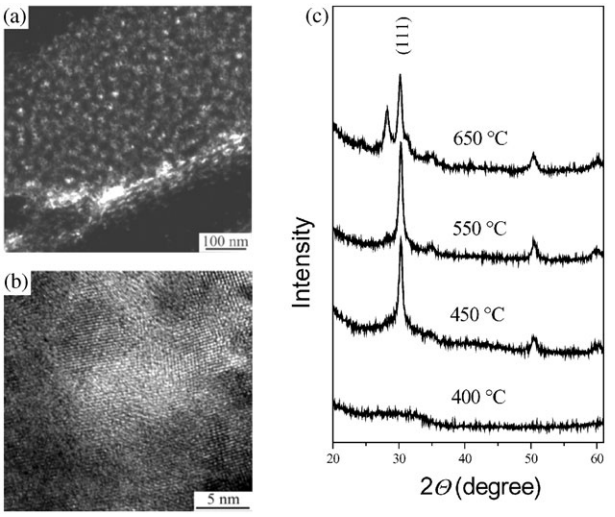

Fig. 4 (a) TEM, (b) HRTEM and (c) WAXS of ZrO_2 thin films (the electron microscopy images were taken of a film treated at 450 °C). The WAXS pattern is consistent with the monoclinic modification of ZrO_2.

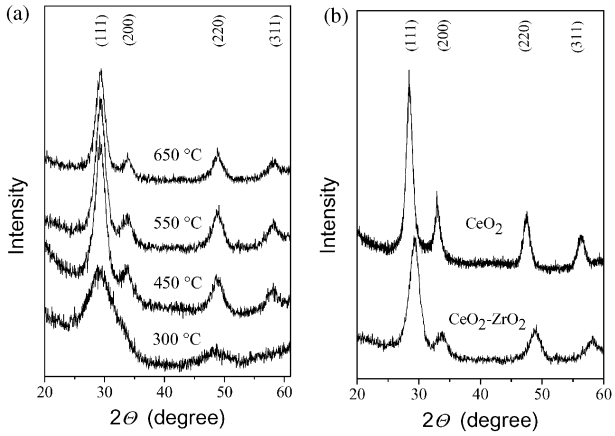

Fig. 6 WAXS diffractograms of the mixed ceria–zirconia species (molar ratio Zr : Ce = 1 : 1). (a) Development of crystallinity as a function of temperature. (b) Comparison between CeO_2 and CeO_2–ZrO_2 mixed oxide films indicating the presence of solid solutions.

recently for other cubic systems.[1a,8] A second-order reflection in the 1D SAXS curves is found even for substantially crystallized samples up to $T = 450$ °C [Fig. 3(a)], suggesting a high degree of mesostructural order. It has to be emphasized that SAXS experiments in reflection on a diffractometer are more sensitive to weak diffraction peaks than the CCD camera used for GISAXS. From the GISAXS and SAXS experiments, we obtain a lattice parameter for the structure of $a = 16$ nm, assuming a distorted bcc structure (see Fig. 3). The relatively large width of the interferences [Fig. 3(a)] is explained by the small film thickness (*ca.* 200 nm), corresponding to only *ca.* 12 layers of pores perpendicular to the surface.

Interestingly, the shrinkage of the mesostructure induced by heat treatment is moderate, because we find an overall uniaxial shrinkage (in the [110] direction) of 20%. It is noteworthy that the lattice parameter of the mesostructure does not change significantly, even up to temperatures of 650 °C (data not shown). Thereby, these mesostructured CeO_2 films show high promise for applications involving even elevated temperatures.

Mesostructured ZrO_2

In order to verify the general applicability of our procedure and to test the other pure counterpart, thin films of ZrO_2 were prepared. Interestingly, the crystallization takes place at about 450 °C, which is significantly higher than for CeO_2. The mesoporous structure is retained but with a more pronounced shrinkage.

As seen in Fig. 4, the mesostructure is not as well-organized as in case of CeO_2. WAXS as a function of temperature [Fig. 4(c)] characterizes the crystallization as a function of the heat treatment. Also, a nanocrystal size of 10 nm (at 450 °C) is obtained from WAXS, being much larger than in the case of CeO_2.

Systems with a primary crystal size of the order of the mesopore size are, in our experience, critically close to possible structural collapse. These mesostructures were also less ordered (see ESI for SAXS) and showed significant unidirectional shrinkage.

Mixtures of CeO_2 with ZrO_2

Mixed oxides of ZrO_2 and CeO_2 were studied with respect to the changes in mesostructure and nanocrystallinity induced by high temperature treatment. Sanchez *et al.* just recently reported that ceria–zirconia thin films can be obtained over a certain range of compositions without phase separation.[8] In the present study, the preparation and crystallization conditions were optimized with respect to the mesostructure quality, in particular with the expectation that a mixed system undergoes slower crystallization because of the formation of solid solutions.

Also in this case, the use of KLE block copolymer as a template provided mesostructured films with crystalline pore walls.

TEM of the symmetric mixed system (tempered at 550 °C) already indicates that this material has a better structural definition and lower shrinkage than the CeO_2 films [Fig. 5(a)]. High resolution electron microscopy of single pores

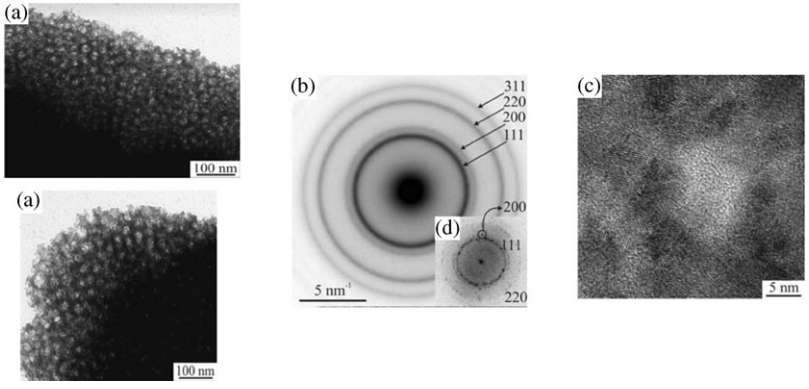

Fig. 5 (a) TEM and (b–d) HRTEM of the CeO_2–ZrO_2 mixed oxide film. (b) HRTEM, selected area electron diffraction of a zone of 250 nm diameter. (c) HRTEM image of a zone of 20 nm side length and (d) the power spectrum.

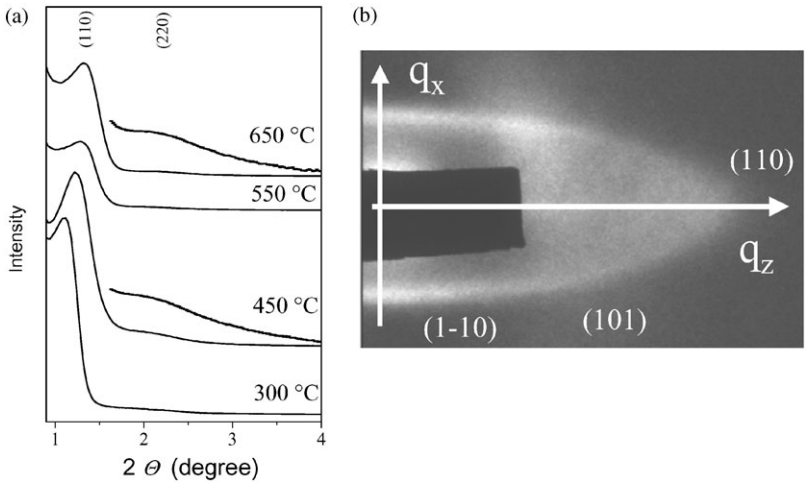

Fig. 7 (a) 1D SAXS and (b) GISAXS (taken at 600 °C) for CeO_2–ZrO_2 thin films. The white shadow in the GISAXS pattern is due to parasitic scattering of the setup.

[Fig. 5(b)] confirms the concept of using mixed oxides for smaller nanoparticles and better mesopore definition: The primary crystal size has dropped markedly compared to ceria to 2–4 nm and each pore is now surrounded/constituted by a larger number of nanoparticles, thus allowing their arrangement around the mesopores and, thereby, replicating the original micelle shape more precisely than in the case of CeO_2. The powder spectrum indicates that the present crystals are indeed solid solutions, that is each crystal is a mixed species. Furthermore, EDX (energy dispersive X-ray) analysis confirmed the 1 : 1 molar ratio between Zr and Ce and the absence of chlorides (also true for CeO_2 and ZrO_2 films).

The crystallization behavior was studied in further detail by WAXS (Fig. 6), revealing important differences compared to CeO_2. First, it is seen that the onset of the crystallization (defined by the observation of the reflections) is shifted to a significantly higher temperature of *ca.* 350 °C. Second, as an important feature for practical applications, this structure does not undergo change even at significantly elevated temperatures; that is the primary mixed nanocrystals keep their size and do not easily recrystallize. Fig. 6(b) compares the WAXS patterns of pure ceria and the mixed symmetric species, both mesoporous and tempered at 550 °C. It is seen that the structures of CeO_2 and CeO_2–ZrO_2 are isomorphous (*i.e.*, cubic fluorite-type), while substitution with zirconia only shifts all peaks to higher angles (cell contraction). Similar results were obtained from mesostructured CeO_2–ZrO_2 films with different Ce/Zr ratios (see ESI). Also, the reflections are broader, confirming the smaller primary particle size (4.5 nm as determined by the Scherrer equation) already observed in electron microscopy. Fig. 7 presents the corresponding SAXS patterns (as a function of the temperature treatment) and GISAXS measurements.

It is noteworthy that even at 600 °C the mixed oxides still show a well-defined mesostructure, which is more defined than in the case of CeO_2. Based on the GISAXS pattern, the primary structure after drying, but prior to crystallization, is indicative of an [110] oriented bcc structure with a lattice parameter of 17 nm (550 °C) or 19.3 nm (450 °C), thus being significantly larger than the one of pure CeO_2. The shrinkage upon crystallization (determined from the positions of the [110] reflection at 300 and 450 °C) is below 10% and recrystallization at higher temperature of the whole structure (usually accompanied with a density increase of about 20%) leaves the mesostructure essentially intact with negligible shrinkage. The overall uniaxial relative shrinkage at 650 °C, compared to 300 °C, is less than 15%, which is attributable to the density change between the amorphous and crystalline states. Note that a film confined to a substrate can only shrink uniaxially, as shrinkage along the other directions would lead to delamination. Compared to other crystalline mesoporous materials, where shrinkages of 60%,[3] 80%,[8] or 40% were obtained,[4] or compared even to our own optimized CeO_2 system (20%), the changes upon crystallization and recrystallization are remarkably small.

Such films, when analyzed either with SEM or AFM (see ESI), turn out to be comparably flat (rms surface roughness of *ca.* 2 nm) and crack- and defect-free. This is much harder to obtain for films that undergo higher shrinkage and sometimes show periodic cracking patterns. The concepts of avoiding the critical size ranges of mesostructures and of making the constituting nanocrystalline elements as small as possible to keep the primary structure have therefore proven valid with these systems.

Conclusion and outlook

In the present study, thin films of mesostructured CeO_2 and CeO_2–ZrO_2 with crystalline pore walls were obtained by evaporation-induced self-assembly (EISA), followed by a suitable thermal treatment. To the best of our knowledge the present study has, for the first time, succeeded in obtaining mesostructured, crystalline CeO_2 films with a well-defined mesopore shape and an overall volume fraction of *ca.* 30–40% porosity. The successful preparation of these materials is attributed to the use of the KLE polymer, which shows several significant advantages compared to the Pluronics polymer family. First, mesostructure formation during dip-coating proceeds substantially faster,[3] thus helping to stabilize the fragile mesohybrid during the metal chloride hydrolysis and, later on, the condensation. Second, the KLE polymer is thermally more stable, thus maintaining the mesostructure even beyond the onset of metal oxide crystallization.

CeO_2–ZrO_2 mixed oxides show an even smaller primary crystal size and a better preservation of the original template structure. This result is in excellent agreement with recent work on CeO_2–ZrO_2 and also demonstrates the absence of surface/thin film effects in the generation of these solid solutions.[12] In particular, it is important to note that the addition of ZrO_2 significantly improves the thermal stability of the films up to a technologically quite appealing region. Future work has to focus on the application of these films for catalytic applications. Also, these films will be the subject to more detailed studies addressing the accessible mesoporosity, lattice defects and the exact redox state of the CeO_2.

Acknowledgements

We are indebted to Dr Heinz Amenitsch (Elletra, Trieste) for experimental support with the GISAXS measurements. Furthermore, we would like to thank Dr David Grosso and Dr Cédric Boissière (Université Pierre et Marie Curie, Paris) for their experimental support and fruitful discussions.

References

1 (*a*) D. Grosso, G. J. D. A. Soler-Illia, E. L. Crepaldi, F. Cagnol, C. Sinturel, A. Bourgeois, A. Brunet-Bruneau, H. Amenitsch, P. A. Albouy and C. Sanchez, *Chem. Mater*., 2003, **15**, 4562; (*b*) E. L. Crepaldi, G. J. D. A. Soler-Illia, D. Grosso, F. Cagnol, F. Ribot and C. Sanchez, *J. Am. Chem. Soc*., 2003, **125**, 9770; (*c*) G. J. Soler-Illia, E. L. Crepaldi, D. Grosso and C. Sanchez, *Curr. Opin. Colloid. Interface Sci*., 2003, **8**, 109; (*d*) E. L. Crepaldi, G. J. D. A. Soler-Illia, D. Grosso and C. Sanchez, *New J. Chem*., 2003, **27**, 9.

2 A. Thomas, H. Schlaad, B. Smarsly and M. Antonietti, *Langmuir*, 2003, **19**, 4455.

3 B. Smarsly, D. Grosso, T. Brezesinski, N. Pinna, C. Boissière, M. Antonietti and C. Sanchez, *Chem. Mater*., 2004, **16**, 2948–2952.

4 D. Grosso, C. Boissière, B. Smarsly, T. Brezesinski, N. Pinna, P. A. Albouy, H. Amenitsch, M. Antonietti and C. Sanchez, *Nature Materials*, 2004, 3787.

5 C. J. Brinker, Y. F. Lu, A. Sellinger and H. Y. Fan, *Adv. Mater*., 1999, **11**, 579–585.

6 (*a*) M. Lundberg, B. Skarman, F. Cesar and L. Reine Wallenberg, *Microporous Mesoporous Mater*., 2002, **54**, 97–103; (*b*) D. Terribile, A. Trovarelli, J. Llorca, C. de Leitenburg and G. Dolcetti, *J. Catal*., 1998, **178**, 299–308; (*c*) J. A. Wang, J. M. Dominguez, A. Montoya, S. Castillo, J. Navarrete, M. Moran-Pineda, J. Reyes-Gasga and X. Bokhimi, *Chem. Mater*., 2002, **14**, 4676–4683; (*d*) D. M. Lyons, K. M. Ryan and M. A. Morris, *J. Mater. Chem*., 2002, **12**, 1207–1212.

7 (*a*) M. Mamak, G. S. Metraux, S. Petrov, N. Coombs, G. A. Ozin and M. A. Green, *J. Am. Chem. Soc*., 2003, **125**, 5161–5175; (*b*) M. Mamak, N. Coombs and G. A. Ozin, *Adv. Funct. Mater*., 2001, **11**, 59–63.

8 E. L. Crepaldi, G. J. D. A. Soler-Illia, A. Bouchara, D. Grosso, D. Durand and C. Sanchez, *Angew. Chem., Int. Ed*., 2003, **42** 347.

9 (*a*) M. Yashima, M. Kakihana and M. Yoshimura, *Solid State Ionics*, 1996, **86**, 1131–1149; (*b*) D. Terribile, A. Trovarellia, J. Llorca, C. de Leitenburg and G. Dolcettia, *Catal. Today*, 1998, **43**, 79–88; (*c*) P. Fornasiero, G. Balducci, R. DiMonte, J. Kaspar, V. Sergo, G. Gubitosa, A. Ferrero and M. Graziani, *J. Catal*., 1996, **164**, 173–183.

10 (*a*) S. Logothetidis, P. Patsalas and C. Charitidis, *Mater. Sci. Eng., C*, 2003, **23**, 803–806; (*b*) M. P. Kapoor, Y. Ichihashi, K. Kuraoka, W.-J. Shen and Y. Matsumura, *Catal. Lett*., **88**, 83–87; (*c*) P. Jasinski, T. Suzuki and H. U. Anderson, *Sens. Actuators, B*, 2003, **95**, 73–77; (*d*) R. Ramamoorthy, P. K. Dutta and S. A. Akbar, *J. Mater. Sci*., 2003, **38**, 4271–4282; (*e*) D. Perednis and L. J. Gauckler, *Solid State Ionics*, 2004, **166**, 229–239; (*f*) P. Patsalas, S. Logothetidis, L. Sygellou and S. Kennou, *Phys. Rev. B*, 2003, **68**, 35104; (*g*) N. Izu, W. Shin, I. Matsubara and N. Murayama, *Sens. Actuators, B*, 2003, **94**, 222–227.

11 (*a*) J. Kaspar, P. Fornasiero and M. Graziani, *Catal. Today*, 1999, **50**, 285–298; (*b*) A. Trovatelli, *Catal. Rev. Sci. Eng*., 1996, **38**, 439–520; (*c*) J. Kaspar, P. Fornasiero and N. Hichkey, *Catal. Today*, 2003, **77**, 419–449.

12 A. S. Deshpande, N. Pinna, P. Beato, M. Antonietti and M. Niederberger, *Chem. Mater*., 2004, **16**, 2599–2604.